Jour. Fac. Sci., Hokkaido Univ., Ser. VII (Geophysics), Vol. 11, No. 1, 265-300, 1998.

Convective and Stratiform Components of Tropical Cloud Clusters in Determining Radar Adjusted Satellite Rainfall during the TOGA-COARE IOP

Md. Nazrul Islam*, Hiroshi Uyeda, Osamu Kikuchi and Katsuhiro Kikuchi

Division of Earth and Planetary Sciences, Graduate School of Science, Hokkaido University, Sapporo 060-0810, Japan

(Received November 30, 1997)

Abstract

This paper describes the estimation of convective and stratiform precipitations from both radar and GMS-IR hourly T_{BB} data during the TOGA-COARE IOP. The CST (Convective Stratiform Technique) algorithm was adapted for TOGA-COARE convection to analyze GMS-IR data in the analysis area (5N-5S, 150E-170E) and compare the results with those of radar analysis.

The convective and stratiform precipitations falling from the MCSs were identified and quantified by radar image after defining a threshold reflectivity of 40 dBZ for Keifu Maru radar. The defined threshold successfully separated the convective and stratiform cloud components. Using the rain rates assigned from Keifu Maru radar data, the CST analysis was performed on the satellite data to obtain good agreement between the results of the two analyses. The convective and stratiform cloud components embedded regions were shown to be about 25% and 75% respectively. The rainfall amounts were calculated at 62% (radar) and 64% (CST) for convective, and 38% (radar) and 36% (CST) for stratiform. These results are strongly consistent with the results of GATE.

Three stages of the tropical clouds were objectively analyzed by using a parameter named length of cloud (L). The length ranges were separated as (1) formative: $L<100$ km; (2) mature: $100<L<330$ km; and (3) dissipating: $L>330$ km.

After obtaining a strong agreement with the radar analysis over a limited coverage of radar, the CST was applied to the entire life history of the tropical clouds and cloud clusters. The CST enabled the extraction of the precipitable portion of the defined cloud (by $T_{BB}=230$ K): 56% of the cloud was precipitable while 44% was nonprecipitable. The surface precipitation determined by radar was 90% of the precipitable portion determined by the CST which demands a strong agreement between the results of radar and CST.

* Present affiliation: Department of Physics, Bangladesh University of Engineering and Technology, Dhaka-1000, Bangladesh

1. Introduction

It is well known that heavy precipitation (3-5 $m \cdot yr^{-1}$) is falling from the tropical convection, especially over the tropical Pacific warm pool, with an ocean surface temperature exceeding 28°C. This is one of the most convectively active regions of the world.

Precipitation from the mesoscale convective systems (MCSs), as typical of the warm pool, has both convective and stratiform components (Houze, 1977; Leary, 1984). However there is no standard way to separate them in radar and satellite images. The MCSs are recognizable by their cloud shields seen in IR satellite pictures. Generally, the cloud clusters are a few hundred kilometers in horizontal dimension (Machado and Rossow, 1993; Uyeda et al., 1995), and the underlying precipitation area is on the order of 10^3 km^2 or more. These cloud clusters as complexes of convection, develop large regions of stratiform precipitation during their lifetimes. It was estimated that 30%-50% of the total rain reaching the ground from such a system is typically stratiform (Leary, 1984; Houze and Hobbs, 1992). It was necessary to divide the convective and stratiform components of the tropical cloud systems; since the dynamics of the air motions and the physics of the precipitation growth in the convective and stratiform regions are fundamentally different. It is also known that shorter duration and low-level convective rainfalls are more intense and are related to the warm rain process (Takahashi and Uyeda, 1995). In the later stage, an updraft above the freezing level produced an anvil cloud which may lead to the long lifetimes of the MCSs. Also produced was light precipitation which is related to the cold rain process. Moreover, for a better understanding of the water budget and to estimate the imported moisture amount over the warm pool, it is necessary to divide the convective and stratiform cloud components into both radar and satellite images. Furthermore, the extraction of the precipitable portion of the cloud is essential for this purpose. For these reasons, it appears to be important that the convective and stratiform regions of MCSs be distinguished, in a domain as large as possible in order to examine the whole life cycle of the system. This will be presented in this analysis.

The stages of the tropical cloud viz; formative, mature and dissipating (Leary and Houze, 1979a; Machado and Rossow, 1993) are well known. These are named on the basis of rough assumptions: the time period of the cloud life, intensity, and size. We need to clarify the particular size and strength of the cloud in each stage in an objective way. This knowledge may be useful in the parameterization of tropical cloud models. This work revealed these prop-

erties by using a large coverage of Keifu Maru C-band radar data in addition to the analysis of satellite data.

Because of the lack of conventional cloud and precipitation observations over the ocean, the use of satellite data is obviously desirable. Recently, Liu et al. (1995) proposed a new cloud classification scheme that uses infrared and microwave satellite data. They tested their algorithm on the tropical convection during the Tropical Ocean Global-Atmosphere program, Coupled Ocean-Atmosphere Response Experiment (TOGA-COARE) Intensive Observation Period (IOP) and obtained general agreement with radar detected large cloud systems. They reported that the new algorithm, however failed to retrieve the shallow, isolated convection wihch produced 61% pixels as nonprecipitating out of 85% while the remaining 15% was precipitating. Generally, a shallow isolated cloud may have a horizontal scale of approximately 5 km and lifetime of approximately 20 minutes which is not detectable by low spatial resolution satellite data as used by Liu et al. (1995). However, the precipitation amount associated with shallow and isolated convection are important in understanding the warmness of the ocean surface because this convection is generally accompanied by low wind speeds and the formation of a fresh water lens on the ocean surface (Webster and Lukas, 1992). Moreover, radar data demands a clear determination of the precipitation amounts associated with shallow and isolated convection. Therefore, the use of radar data to calibrate the results of high spatial resolution satellite data will result in the classification and quantification of all types of clouds in the tropics. Performing the calibration where radar data is available will be useful for a large domain using only satellite data. The present work focuses on the radar adjusted satellite precipitation by using high temporal and spatial resolutions of GMS-4 data in addition to radar data to obtain the general agreement between the results of two data sets.

Adler and Negri (1988; hereafter AN88) proposed and Goldenberg et al. (1990; hereafter GHC90) modified a technique that uses geosynchronous IR data to distinguish between the convective and stratiform components of mesoscale convective cloud systems that have extensive cirriform tops. AN88 tested their algorithm, referred to as the Convective Stratiform Technique (CST) on the Florida convection, and obtained general agreement with radar and rain-gauge observed rainfall. GHC90 tested their modified CST on the cloud cluster B (referred by Churchill and Houze, 1984a) observed during the Winter Monsoon Experiment (WMONEX). They calculated 38% as convective and 62% as stratiform rainfalls for the total lifetime of the cloud cluster B. They obtained,

furthermore, similar results of radar value at the early period, before the system moved out of range of the coastal radar. Kikuchi and Uyeda (1996) applied the GHC90's CST on the cloud clusters observed in Manus Island during the TOGA-COARE IOP. They reported disagreements between the results of radar and the CST. This implies that the properties of the convection in the TOGA-COARE domain are somewhat different from the properties of Florida convection or WMONEX convection. To make certain that the TOGA-COARE convection differs from the Florida or WMONEX convection, recently, Islam et al. (1996, 1997) tested again the GHC90's CST on data from the GMS-4 and compared the results with that of Keifu Maru radar data collected in the Intensive Flux Array (IFA) region during the TOGA-COARE IOP. They found good agreement between the areas determined by the CST and radar, however reported disagreement between the rainfall amounts determined by the CST and radar. They strongly recommended the necessity of the modification of the CST for the TOGA-COARE convection. Therefore, it will be a sophisticated task to adapt the CST for the analysis of GMS-4 data to obtain a comparable result with that of radar. The main purpose of the use of the CST in the present study is to adapt it for TOGA-COARE domain and analyze the horizontal precipitation structure (area and rainfall amounts) of cloud clusters by using GMS-4 IR data in the IFA region over the western Pacific warm pool.

2. Data

The research vessel "Keifu Maru" carried a C-band (wavelength: 5 cm) conventional weather radar covering 250 km in radius collected data in the IFA region as shown in Fig. 1. The outline of the Keifu Maru radar system is described in Mori (1992). The ship track of the Keifu Maru on the TOGA-COARE cruise is described in Mori (1995). Reflectivity data digitized over a 2.5 km mesh was obtained over a 500 km $\times$ 500 km area covering a large part of the IFA. During the observation period (Nov. 3-16, 1992), 3 level (0.0°, 0.7° and 1.4°) PPI (Plan Position Indicator) scan data every 7.5 minutes, and 10 level (0.4°-14.4°) PPI data every one hour was stored on magnetic tapes. The 7.5 minutes interval PPI data with elevation angle of 0.0° from Nov. 3-12, 1992 was utilized in the present study.

The GMS-4 data (on CD-ROM), with the 0.1° mesh, over the TOGA-COARE domain were utilized. The GMS data was provided by Dr. Nakazawa, Meteorological Research Institute, Japan Meteorological Agency (JMA). The hourly GMS-IR data was specially processed for TOGA-COARE IOP by JMA

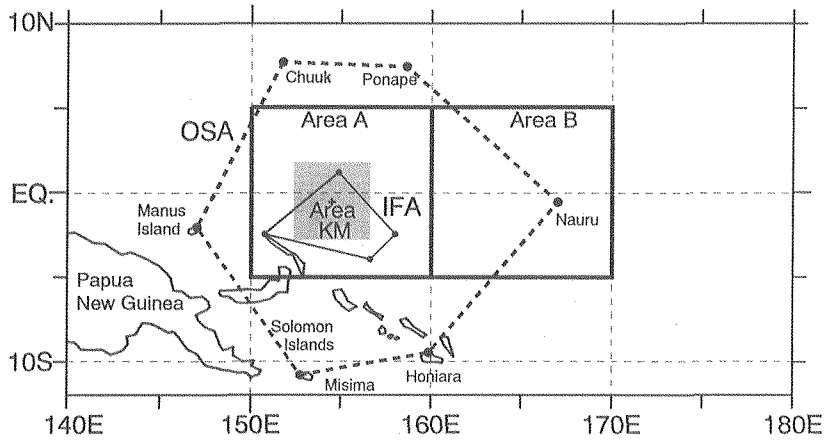

Fig. 1. Location of the radar observation in the TOGA-COARE domain. The outer sounding array (OSA) and the intensive flux array (IFA) are outlined. The Keifu Maru is located at the northern part of IFA denoted by the + mark. The shaded area indicates the domain of the Keifu Maru (Area KM). Heavy solid lines represent two analysis areas named Area A (5N-5S, 150E-160E) and Area B (5N-5S, 160E-170E).

and was used for this analysis.

3. Methods of analysis

3.1 Modification of convective stratiform technique (CST)

Details of the analytical procedure of the CST are described in AN88, GHC90, Kikuchi and Uyeda (1996). As discussed in Islam et al. (1997), the comparative results of radar and CST suggested a need to check the CST algorithm for TOGA-COARE domain. Some simple and essential modifications were performed on the CST algorithm to adapt the CST for the TOGA-COARE convection.

a) Slope parameter

In order to identify the locations of convective cores in each satellite image, the IR T_{BB} field was examined for relative minima (T_{min}). It may be either a single pixel minima or the centroid of a multi pixel minima in a square box of 50 km×50 km. After identifying the pixel location of T_{min}, its strength was measured by calculating the slope parameter (S). In this way all of the points colder than their respective environments are regions of enhanced convection. No minima warmer than 240 K are considered in this study. The strength of

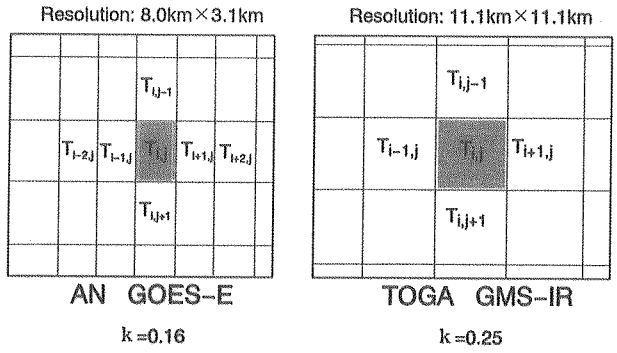

Fig. 2. Schematic illustration of satellite grid resolutions as used by AN (1988) for GOES-E and in this analysis for TOGA by GMS-IR. The constant k represents the value to use in equation (1) of the text.

the slope parameter determines the candidate $T_{\min}$ pixel as convective or not. In this study four surrounding pixels were involved instead of six surrounding pixels (AN88 ; GHC90) in calculating the slope parameter. The variation of pixel number depends on the resolution of satellite data which is used. The slope parameter equation adopted is

$$S=k(T_{i-1,\ j}+T_{i+1,\ j}+T_{i,j-1}+T_{i,\ j+1}-4\,T_{i,\ j}) \tag{1}$$

where S is the slope parameter and i and j refer to the position of the pixel for which S is being calculated. The factor k depends on the data resolution as shown in Fig. 2. In the present study $k=0.25$ for four surrounding pixels of GMS-4 (11.1 km×11.1 km) while it was $k=0.16$ for six surrounding pixels of GOES-E (8 km×3.1 km) used by AN88.

b) Fit for x value

According to GHC90, the stratiform threshold temperature Ts is given by

$$Ts(^{\circ}\mathrm{K})=T_{\mathrm{mode}}+x \tag{2}$$

where T_{mode} is the modal temperature, x is a variable introduced by GHC90 and in their case $x=7$ K. The necessity of introducing the variable x depends on the usage of radar reflectivity to be compared with the results of the CST analysis. AN88 excluded all echoes <25 dBZ of Miami radar, whereas GHC90 included all echoes ≥ 1 dBZ of MIT land-based radar. The need for the addition of $x=7$ K was obtained by GHC90 for their case rather than $x=0$ K for AN88. The present study excluded all echoes <20 dBZ of Keifu Maru radar in avoiding sea clutters. In this study $x=4$ K was found to be a good fit for short-

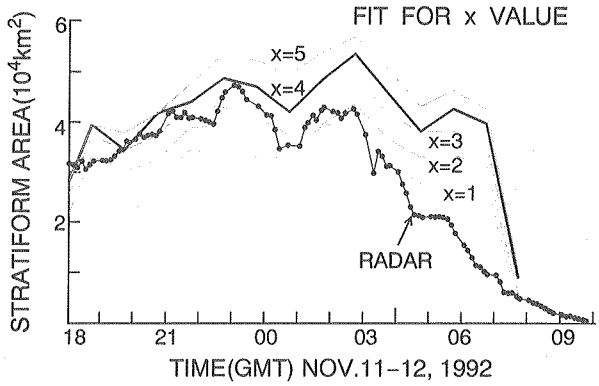

Fig. 3. Time sequence of the area covered by stratiform precipitation as determined by CST application (x values) and Keifu Maru radar analysis (RADAR) on Nov. 11-12, 1992.

term (<1 day) analysis and $x=7$ K was good fit for long-term (10 days) analysis. The fit for x value for short-term analysis is shown in Fig. 3. This figure compares the CST derived stratiform precipitation areas as determined by equation (2), for $x=1$, 2, 3, 4, and 5 K, with the Keifu Maru derived stratiform precipitation areas. It would be expected that the CST derived areas, if "correct", should almost always be equal to or greater than the radar derived areas, and never less. Using this criterion, the closest overall satellite-radar match in Fig. 3 is for $x=4$ K.

c) Rain rate

AN88 determined the relationship between convective precipitating regions (cores) and cell top height, which is indicated by cloud top height, from the results of a one-dimensional model output used by Adler and Mack (1984) for Florida convection. To adjust the resolution of the one-dimensional model (1 km^2) and GOES-E data (8 km×3.1 km), AN88 decided to apply the correction for cloud top temperature of relative minima, $T_{\min}$, associated with a convective core, as follows:

$$T_{\min}-T_C(^\circ\mathrm{K})=\begin{cases}0.283\,T_{\min}-56.6, & (T_{\min}>200\ \mathrm{K})\\ 0, & (T_{\min}\leq 200\ \mathrm{K})\end{cases} \tag{3}$$

where T_C is corrected temperature. GHC90 divided the r.h.s of equation (3) by 2.5 to adjust with GMS-1 data resolution (5.2 km×2.1 km). This implies the need to multiply the r.h.s of equation (3) by about 5 to adjust with the present data of GMS-4 on CD-ROM in the resolution of 11.1 km×11.1 km. However,

the same relation of AN88 was adopted in this analysis, because the multiplication of r.h.s in equation (3) by 5 makes no sense on the condition $T_{min}>200$ K.

Now the relation of convective rain rata R_C as a function of T_C is given by

$$\ln(R_{Ci})=eT_{Ci}-f \tag{4}$$

where i refers to the i-th core and $e=-0.0175$, $f=4.76$.

The value of R_C obtained in the present analysis is nearly 5 mm·h^{-1}, which is the same as calculated by Islam et al. (1996), while GHC90 calculated 3-7 mm·h^{-1} and AN88 calculated 20 mm·h^{-1}.

At present there is no standard way to calculate a reasonable rain rate using only satellite data. Moreover, there is no way to evaluate the stratiform rain rate from the CST algorithm. AN88 assigned it in arbitrary way and used 2 mm·h^{-1} assuming one-tenth of the mean convective rain rate (20 mm·h^{-1}). They calculated the convective rain rate using the CST itself with the help of a one-dimensional cloud model (Adler and Mack, 1984). GHC90 followed AN88 in calculating the convective rain rate and assumed the stratiform rain rate (2 mm·h^{-1}) from radar data. The recent analytical results described in Islam et al. (1997) clearly showed the disagreement between the rain rates determined by the CST and radar for the TOGA-COARE data, and strongly suggested the need to assign the CST rain rate from radar data. In the present analysis, 3.5 mm·h^{-1} and 25 mm·h^{-1} were assigned as the stratiform and convective rain rates respectively, which are the average values of below and above 11.53 mm·h^{-1} (= 40 dBZ) for Keifu Maru radar. This assigned value for stratiform rain rate was consistent with the result of Rappaport (1982) 3.3 mm·h^{-1} and comparable to the result of Gamache and Houze (1983) 2.6 mm·h^{-1}. The convective rain rate assigned from Kedfu Maru radar was comparable to the calculated value of AN88. The detailed procedure of the assignment of convective and stratiform rain rates will be described in the next sections *3.2* and *4.2*.

3.2 Assignment of area and rain rate from radar data

a) Definition of a threshold reflectivity to divide convective and stratiform components

As a ground truth device, radar is reliable in assigning the rain rate. However, there is no particular way to divide them into convective and stratiform components in radar image. Therefore, to extract convective from stratiform cloud component, it was necessary to draw a discrimination line which was able to separate the convective and stratiform components from each other in a radar image. The discrimination line was defined by a particular

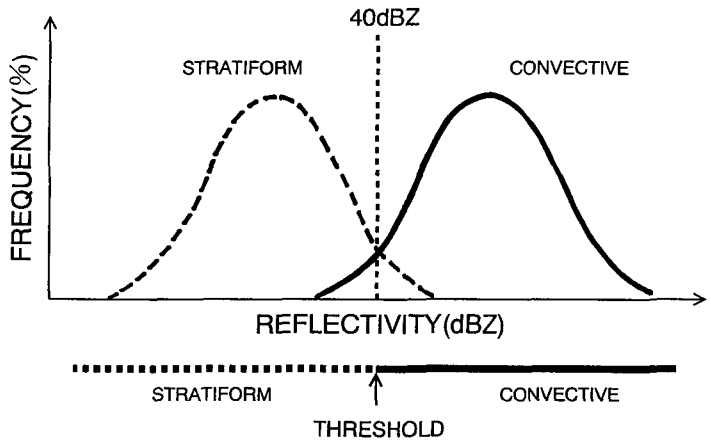

Fig. 4. Schematic illustration on the definition of convective and stratiform cloud components for radar analysis. A particular threshold is determined (40 dBZ) to discriminate convective and stratiform components in the radar PPI image.

threshold reflectivity like the schematic diagram of Fig. 4. In general, a stratiform component has to be low intensity while a convective component has to be relatively high intensity. The occurrence frequency of stratiform and convective components is shown against threshold values (Fig. 4). All of the pixels in a PPI scan which were above a particular threshold (i.e., 40 dBZ) were the status of stratiform. Those pixels above the threshold were the status of convective. Using this assumption, this analysis separated the components by identifying a threshold reflectivity which was 40 dBZ for Keifu Maru radar. Here a few stratiform pixels were considered in the convective region.

b) Radar rain rate

After determining the threshold value to separate the convective and stratiform areas, it was decided that reflectivity be converted into rain rate by using the Z-R relationship. This analysis adopted the standard Z-R relationship given by

$$Z = BR^{\beta} \tag{5}$$

where Z is the radar reflectivity factor in $mm^6\ m^{-3}$, and R is rain rate in $mm \cdot h^{-1}$, and B and β are positive numbers determined empirically. The value of B varies over a range of few hundred units (e.g., Battan, 1973). The factor β on the other hand, is microphysically limited to the range of $1 \leq \beta \leq 3$ (Smith, 1993). According to Marshall and Palmer (1948) the factors B and β are 200 and 1.6,

respectively for rainfalls in this analysis. The Z-R relationship can be used in a variety of forms after changing the values of B and β which are determined by the size distribution of precipitation particles. For examples, Woodley (1970) used $B=300$ and $\beta=1.4$ for FACE, Austin (1976) used $B=230$ and $\beta=1.25$ for GATE, Steiner et al. (1995) used $B=167$ and $\beta=1.25$ for Darwin. Furthermore, separate Z-R relations are determined and applied to the convective and stratiform areas by Steiner and Houze (1993), Steiner et al. (1995). Steiner and Houze (1993) used $B=50$ and $\beta=1.5$ for convective, and $B=115$ and $\beta=1.5$ for nonconvective (stratiform) precipitation. Steiner et al. (1995) used $B=82$ and $\beta=1.47$ for convective, and $B=143$ and $\beta=1.5$ for nonconvective (stratiform) precipitation. It was difficult to determine which was the particular Z-R relationship, therefore, by selecting one, rain rate was calculated and the result was compared with the results of satellite analysis. The most popular values of 200 and 1.6 for B and β respectively were adopted.

The rain rate obtained from the average value of >40 dBZ ($=11.53$ mm·h^{-1}) in a PPI scan was used as the convective rain rate (R_C) of this study. The moderate stratiform rain rate (R_S) was used as the value obtained after subtracting the average value of ≥ 20 dBZ from R_C in the same PPI scan. The actual stratiform rain rate was calculated from the average rain rate ≤ 40 dBZ in a PPI scan. The determination of 40 dBZ as a threshold reflectivity to divide convective and stratiform components will be described in section *4.2*.

c) Definition of length (L) of echo and cloud

The length (L) of echo and cloud was calculated from the circumference of an equivalent area circle given by $L=2\pi r$, where r is the radius of an equivalent area circle which can be used to calculate the size of a cloud (Machado and Rossow, 1993). The length was used to measure objectively the echo and cloud areas ($A=L^2/4\pi$) in the different stages of the tropical cloud.

4.1 A few active convective events

During the study period (Nov. 3-12, 1992), four active periods having 1-3 day activities were analyzed as shown in Fig. 5. In each active period there were two or more peaks indicating the occurrence of successive convection during that period. The labels in the upper panel represent the particular threshold reflectivity below which the area was calculated. The corresponding cloud area identified by GMS-IR and the CST identified area are shown in the middle and lower panels respectively. The lables for the middle panel are the same as the upper panel except for particular T_{BB} instead of reflectivity. The thin vertical lines are drawn to show the peak differences among the three panels. It is

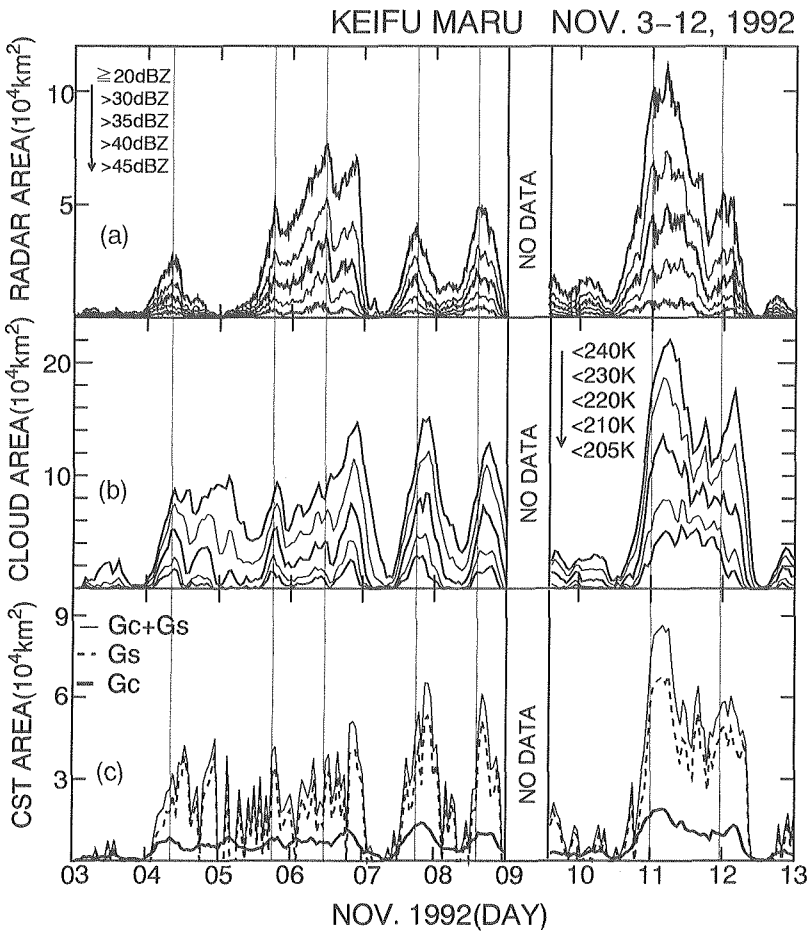

Fig. 5. Time sequences of the area covered by a) Total echo, b) Cloud, and c) CST determined regions. The levels are for a) threshold reflectivity, b) threshold T_{BB}, and c) stratiform (Gs) and convective (Gc) rainfall amounts.

obvious that the peaks of the cloud area and CST identified area are almost coinciding. The peaks of the radar echo area were 2-4 hours (average 2 hours) earlier than the peaks of cloud and CST areas. It is also seen that the peak of very cold cloud area (<210 K) was very close to the peak of the radar echo area (e.g., 0800 GMT on Nov. 4, 1500 GMT on Nov. 5 and 1500 GMT on Nov. 7). Moreover, the CST identified curves especially for stratiform (G_S) were very pulsating in nature because they varied with small changes of T_{BB}. The up-down of the convective (G_C) and G_S areas identified by the CST were significant

in realizing the internal structure of clouds. This result as shown in Fig. 5 was used in calculating precipitation in the next section *4.2*.

4.2 A threshold reflectivity for Keifu Maru radar to divide convective and stratiform components

To date there is no standard method for dividing convective and stratiform precipitation areas in radar and satellite images. Due to this lack of a standard method, the process of divding these has depended on the researcher. According to Leary (1984), 4 km×4 km bin was used for either convective or stratiform depending on the strength of the reflectivity. He used cell top height. Convective cells are characterized by high radar reflectivities (Cheng and Houze, 1979), sharp horizontal gradients in reflectivity and frequent overshooting echo tops. On the contrary, stratiform precipitation is characterized by lower reflectivities, weaker horizontal gradients of reflectivity and more uniform echo top height than convective precipitation. Precipitation areas larger than 100 km^2 frequently contain regions of stratiform and are accompanied by convective cells (Leary, 1984). According to Steiner and Houze (1993), a 10 km×10 km box of reflectivity field is considered convective if any data point of 2 km×1.5 km grid pass the convective criteria. The use of a whole 10 km resolution grid box as a convective echo even when only one data point is convective sometimes may not be applicable for an individual, shallow convective cloud, because an individual shallow convective cloud may have a horizontal scale of 5 km and a lifetime of 20 minutes (Liu et al., 1995). Recently, Williams et al. (1995) proposed an algorithm that classifies precipitating clouds into its components using the vertical structure of reflectivity, velocity and spectral width derived from measurements made with the Doppler wind profiler at Manus Island. However, this analysis has no RHI scan data for Keifu Maru radar to see the vertical structure and is not able to calculate cell top height. Therefore, it was decided that the strength of radar reflectivity be used to divide convective and stratiform components and a positive agreement with the other research results was found.

With the knowledge of the characteristics of MCSs, it is clear that a proper threshold to divide convective and stratiform cloud components is needed to estimate rainfall from satellite data. It is a difficult task to assign a proper threshold and at present it is not known which is the absolute threshold value ; but a comparable value is needed and useful. To determine this, rainfall amounts were calculated from radar and satellite data and tabulated at five thresholds as in Table 1. It is seen that the convective rainfall amount deter-

Table 1. Rainfall amounts estimated by radar and CST analyses for 10 days from November 3, 1992. The convective rain rate determined by the CST is used to calculate the CST convective rainfall amount. The moderate stratiform rain rate is used to calculate the CST stratiform rainfall amount.

	RADAR (10^{13} kg)					CST (10^{13} kg)					RATIO (%)				
THRESHOLD (dBZ)	35	38	40	42	45	35	38	40	42	45	35	38	40	42	45
CONVECTIVE	3.65	3.2	2.8	2.3	1.6	0.6	0.6	0.6	0.6	0.6	608.3	533.3	466.7	383.3	266.7
STRATIFORM	0.85	1.3	1.7	2.2	2.9	3.5	5.1	6.6	8.5	8.8	24.29	25.49	25.76	25.88	32.96
TOTAL	4.5	4.5	4.5	4.5	4.5	4.1	5.7	7.2	9.1	9.4	109.8	78.95	62.5	49.45	47.87

Table 2. Same as Table 1 except for convective rain rate assigned from radar is used to calculate the CST convective ainfall amount.

	RADAR (10^{13} kg)					CST (10^{13} kg)					RATIO (%)				
THRESHOLD (dBZ)	35	38	40	42	45	35	38	40	42	45	35	38	40	42	45
CONVECTIVE	3.65	3.2	2.8	2.3	1.6	2.1	2.9	3.1	3.9	5.0	173.8	110.35	90.32	58.98	32.0
STRATIFORM	0.85	1.3	1.7	2.2	2.9	3.5	5.1	6.6	8.5	8.8	24.29	25.49	25.76	25.88	32.96
TOTAL	4.5	4.5	4.5	4.5	4.5	5.6	8.0	9.7	12.4	13.8	80.26	56.25	46.39	36.29	32.61

mined by the CST was much lower than that of radar. In contrast, the stratiform rainfall amount determined by the CST was much higher than that of radar. The third row of Table 1 shows that the ratios for convective rainfall amounts were unexpected. It should be noted that convective rain rate calculated by the CST algorithm is used in this calculation. To get adjusted and desired values of convective rainfall amount determined by the CST, there is one way to use the radar convective rain rate as the CST convective rain rate for the rainfall calculation. New estimated rainfall amounts are tabulated in Table 2. The third row of Table 2 shows that the reasonable adjustment started at the threshold of 40 dBZ. The adjustment criterion was based on the assumption that the rainfall amount determined by satellite would be greater than that of radar. For a better understanding, the graphical representation of Table 2 is shown in Fig. 6.

As shown in Fig. 6, it is obvious that the threshold reflectivity for Keifu Maru radar was almost 40 dBZ, because at this threshold, the convective rainfall amount determined by the CST started to measure a higher amount than that of radar. In other words, the threshold reflectivity of 40 dBZ passed the criterion to adjust the rainfall amounts determined by the CST with that of radar. Below 40 dBZ, the CST estimated value was lower than that of radar. Simple calculation showed that radar determined convective and stratiform rainfall

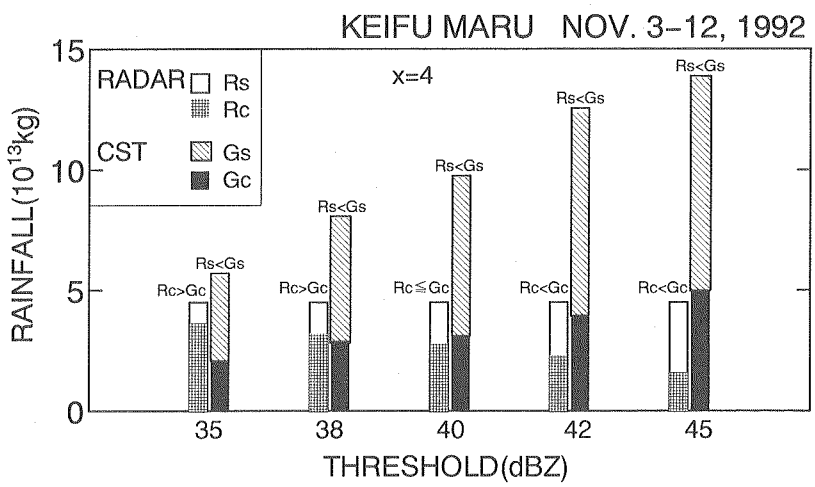

Fig. 6. Total rainfall amounts of 10 days (Nov. 3-12) calculated by Keifu Maru radar and CST analyses. The legends are shown in the upper left corner for both radar (R) and for the CST (G) analyses. The subscripts s and c are used for stratiform and convective components at a particular threshold reflectivity.

amounts were 62% and 38% respectively, at the threshold of 40 dBZ. The rainfall amount for the stratiform component was consistent with the result of Houze (1977) who calculated 40% for GATE (Global Atmosphere Research Program's Atlantic Tropical Experiment) case. The CST determined convective and stratiform rainfall amounts were 32% and 68% respectively, while GHC90 calculated that convective rainfall amount was 38% and stratiform rainfall amount was 62% for WMONEX. These percentages were opposite the percentages of radar values. GHC90 reported that their calculated stratiform rainfall amount (62%) was somewhat overestimated either by uncalibrated stratiform threshold temperature or by reasons undetermined. However, this analysis estimated that the CST rainfall amount was 2.15 times the radar estimated rainfall amount. The task here is to find out the reason for this overestimation in the calculation of satellite rainfall amount.

By studying ten days data the overestimation of the CST stratiform rainfall amount was found to come from the use of a moderate stratiform rain rate R_S which was too high. Using $x=4$ K which was adjusted for short-term (<1 day) analysis (Fig. 3) resulted in an underestimation of the CST area-time-integrated value for long-term (10 days) data analysis. Use of the high value of R_S in the rainfall estimation was necessary. After the adjustment of long-term data, x value was decided at $x=7$ K and the radar original stratiform rain rate (average

Table 3. Same as Table 2 except for both convective and stratiaform rain rates assigned from radar are used to calculate the CST rainfall amounts.

	RADAR (10^{13} kg)					CST (10^{13} kg)					RATIO (%)				
THRESHOLD (dBZ)	35	38	40	42	45	35	38	40	42	45	35	38	40	42	45
CONVECTIVE	3.6	3.2	2.8	2.3	1.6	2.2	2.7	3.2	3.9	5	165.91	116.36	*87.5	58.97	32.00
STRATIFORM	0.9	1.3	1.7	2.2	2.9	$x=4$ 0.9	1.2	1.4	1.7	2.0	*94.44	108.33	121.48	129.41	141.46
						$x=6$ 1.1	1.4	1.7	2.0	2.4	73.91	*89.65	100.00	110.00	118.37
						$x=7$ 1.2	1.6	1.8	2.2	2.7	68.00	81.25	*94.44	100.00	107.40
						$x=8$ 1.3	1.7	2.0	2.4	2.9	65.38	58.82	85.00	*91.66	100.00
						$x=9$ 1.4	1.8	2.2	2.5	3.1	60.71	72.22	77.27	86.27	*93.54
TOTAL	4.5	4.5	4.5	4.5	4.5	$x=4$ 3.1	3.9	4.6	5.6	7.0	146.16	113.92	*97.83	80.36	63.83
						$x=6$ 3.3	4.2	4.9	5.9	7.4	134.33	107.14	*91.84	76.27	60.40
						$x=7$ 3.4	4.3	5.0	6.1	7.7	130.43	103.45	*90.00	73.77	58.44
						$x=8$ 3.5	4.4	5.2	6.3	7.9	128.57	101.12	*86.54	71.43	56.96
						$x=9$ 3.6	4.5	5.4	6.5	8.1	125.00	*98.9	83.30	69.77	55.55

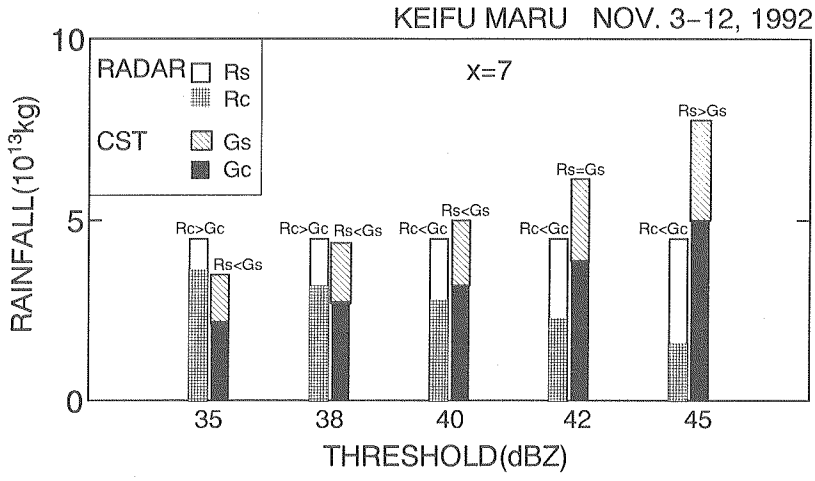

Fig. 7. Same as Fig. 6 except for $x=7$.

3.5 mm h^{-1}) was used to the rainfall calculation. Newly adjusted values are tabulated in Table 3. The convective and stratiform values determined by radar remain the same as in Table 2. The stratiform value determined by the CST is shown for different values of x. The asterisk sign represents when the adjustment starts. Careful examination of Table 3 shows that the threshold of 40 dBZ was better for dividing convective and stratiform cloud components, and $x=7$ K was a good fit for long-term analysis. Steiner and Houze (1993) also used 40 dBZ as an absolute convective threshold for NOAA/TOGA C-band Doppler radar. The graphic representation of Table 3 is shown in Fig. 7. At the threshold of 40 dBZ and $x=7$ K, the CST estimated convective (G_c) and stratiform (G_s) rainfall amounts were 3.2×10^{13} kg and 1.8×10^{13} kg respectively. Calculation shows that $G_c=64\%$ and $G_s=36\%$. These results are much closer to the results of the radar analysis at the same threshold. The stratiform rainfall amounts are well consistent with the results of Liu et al. (1995) who calculated them to be 36% and Cheng the Houze (1979) who calculated them at 35%. In this analysis, the CST calculated rainfall amount was 1.11 times of radar rainfall amount. This agreement strongly suggests the applicability of satellite data to estimate rainfall in a wide area which is not possible by either radar or rain-gauge. Therefore, the threshold of 40 dBZ was used safely and confidentially for Keifu Maru radar data to divide convective and stratiform cloud components. The assigned rain rate with this threshold is used in the CST algorithm to analyze satellite data in the rest of this analysis.

4.3 Classification of rain regimes in an objective way

Rainfall regimes can be classified into three categories viz ; a) formative, b) mature, and c) dissipating, by using the echo length and the threshold rain rate.

Figure 8 shows the distributions of echo area divided into three length ranges viz ; formative : $L<100$ km ; mature : $100<L<330$ km ; and dissipating : $L>330$ km. On the basis of intensity, formative : $R>25$ mm·h^{-1} ; mature : $17.5<R<25$ mm·h^{-1} ; and dissipating : $R<17.5$ mm·h^{-1} ; where 25 mm·h^{-1} and 17.5 mm·h^{-1} were the average values of convective and moderate stratiform rain rates respectively.

In the formative stage, only the convective component had a predominant small echo length (L) and a strong rain rate confirmed the warm rain (Takahashi and Uyeda, 1995). The warm rain was associated with the individual shallow, convective clouds which lay below freezing level, with no ice phase expected. In the mature stage, both convective and stratiform components were almost equally dominant. This stage appeared to be a mixture of

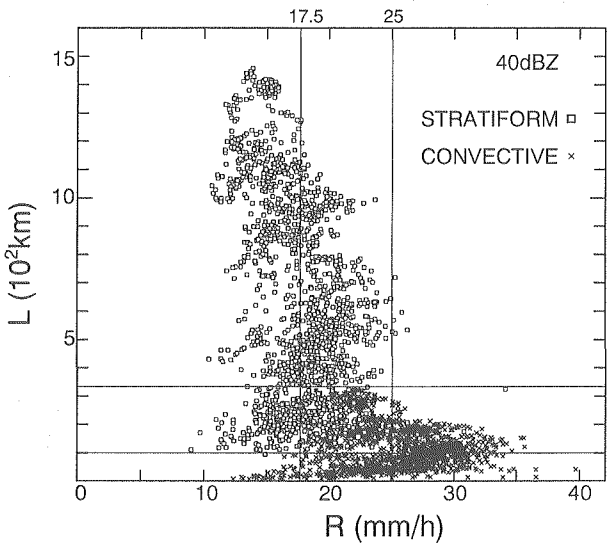

Fig. 8. Comparison of the echo length L represented by the circumference of an equivalent area circle versus rain rate. The convective and stratiform components are separated using the threshold of 40 dBZ. The horizontal and vertical lines are used to divide three stages explained in the text.

convective and stratiform components, so liquid and ice phases were almost equal. The strong and weak rain rates correspond to the convective and stratiform components respectively. From the dissipating stage, large echo length and weak rain rate were analyzed. These implied the production of anvil clouds which brought a large amonut of rain associated with the cold rain process. In this stage most of the rain is expected to have an ice phase. A few echoes having small echo length existed in the formative stage. Actually these were stratiform components in the dissipating stage with relatively high intensity.

One may easily estimate the echo areas in the formative, mature and dissipating stages from their respective echo length. Calculation showed that the maximum echo area ($L^2/4\pi$) at different stages were, formative: $\sim$800 km^2; mature: $\sim$8600 km^2; and dissipating: $\sim$174300 km^2, respectively.

4.4 Cloud size distributions

The area frequency was objectively calculated by using Keifu Maru radar data to measure the fractional coverage of convective and stratiform regions within the total coverage as shown in Fig. 9. The letters T, S, and C represent the total echo area, stratiform area, and convective area respectively. The determined maximum fractional coverages were convective region 11% and stratiform region 34%, out of the total 45%. Here the ratio of convective to stratiform was almost 1 : 3 (=25% : 75%). Examination of scans (20 PPI scans) showed that C/T was 22.2% and S/T was 77.8%. These results show that convective components accompanied almost one-fourth of the total coverage while the rest was accompanied by stratiform components. Machado and Rossow (1993) also reported the fractional coverage of 20% occupied by the convective region in the mature stage of tropical clouds.

Figure 10 represents the area frequency calculated at different threshold reflectivity using Keifu Maru radar data. The rain rate is plotted in reverse axis for the convenience of comparison with the result of CST analysis. For convective ($>$40 dBZ), the area frequency increased gradually with the decrease of the rain rate associated with the warm rain. For stratiform ($\leq$40 dBZ), the area frequency increased rapidly with the decrease of the rain rate associated with the cold rain. This rapid increase makes a linear relationship between the area frequency and rain rate. This is an indication of the production of stratiform anvil clouds. The same linear relationship was observed by GMS data which will be described in Fig. 11.

The distribution of area frequency of the clouds identified by GMS-IR in

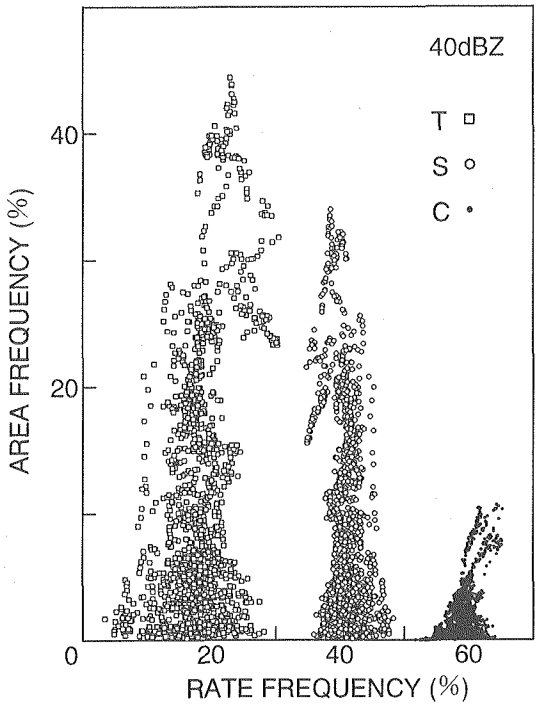

Fig. 9. Area frequency versus rate frequency distribution for total (T), stratiform (S), and convective (C) clouds. The 40 dBZ is used to separate convective and stratiform components.

Area KM is shown in Fig. 11. The cloud area calculated at the different threshold T_{BB} are labeled in the Fig. 11. It is seen that the area frequency was linearly related to the T_{BB} represented by the solid line. Area B was analyzed similarly, as shown in Fig. 12. One of the large clusters is identified by a thin line. In comparison with the area frequency calculated from radar data (Fig. 10), it is clear that the satellite identified area frequency is similar to the stratiform part of the radar identified area frequency. Satellite images are not able to identify the convective part which is well identified by radar. The same conclusion is reported by Liu et al. (1995) stating that, satellite images cannot identify warm precipitaing shallow clouds well. This is why calibration is performed on the precipitation determined by the satellite with the precipitation determined by radar to obtain comparable amounts.

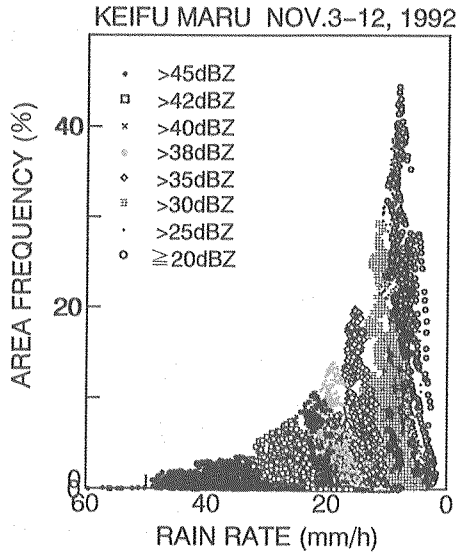

Fig. 10. Same as Fig. 9 except for different threshold reflectivities as labeled in the figure.

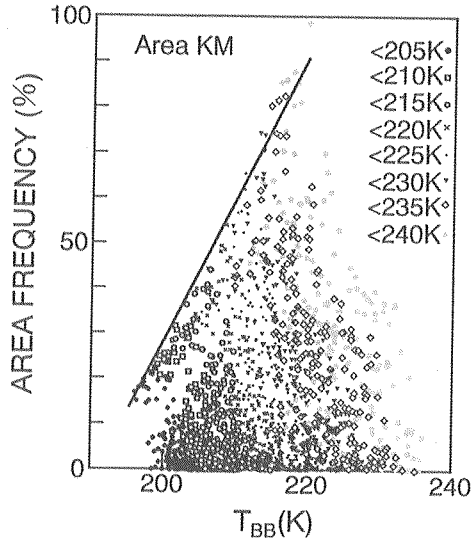

Fig. 11. Area frequency distribution for clouds identified by GMS-IR at different threshold T_{BB} in Area KM. The solid line represents the linear relationship between area frequency and T_{BB}.

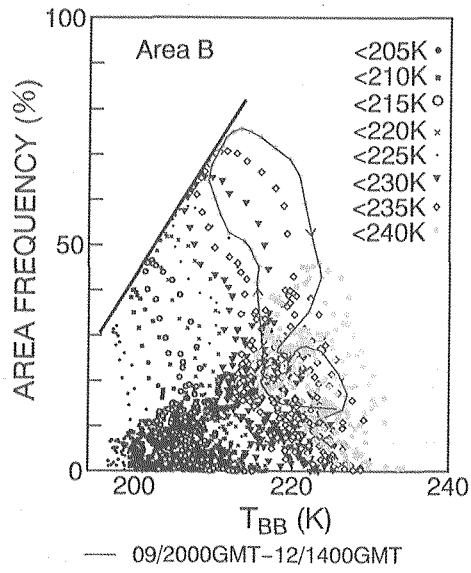

Fig. 12. Same as Fig. 11 except for Area *A*.

4.5 Diurnal variation of the convective activities in IFA region

In this section, diurnal variation of tropical convection is investigated using radar and GMS-4 data. Areal coverages of radar and satellite images are used in terms of cloud amounts. These are very helpful in accounting for which cloud component results the occurrence of the maximum enhancement comes from. The advantage of this analysis is that it uses separated convective and stratiform cloud components. The shallow convective and stratiform cloud bears some information individually.

As shown in the upper panel of Fig. 13, three peaks named P1, P2, and P3 of the echo/cloud area were analyzed. These peaks correspond to the local time 13-16 LST (LST=GMT+10 hours), 01-04 LST, and 05-09 LST respectively. P1, P2, and P3 were the evening peak, early morning peak, and late morning peak respectively. The GMS data analysis also showed three peaks P1, P2, and P3 with a small difference in magnitude and in time duration as represented in the lower panel of Fig. 13. It is obvious that the magnitude of P2 was large for a radar identified area and the magnitude of P3 was large for a CST identified area. These are interesting and important aspects in analyzing the cloud properties in the lower troposphere (radar) and upper troposphere (CST).

Radar analysis shows the maximum peak in the early morning (P2), after

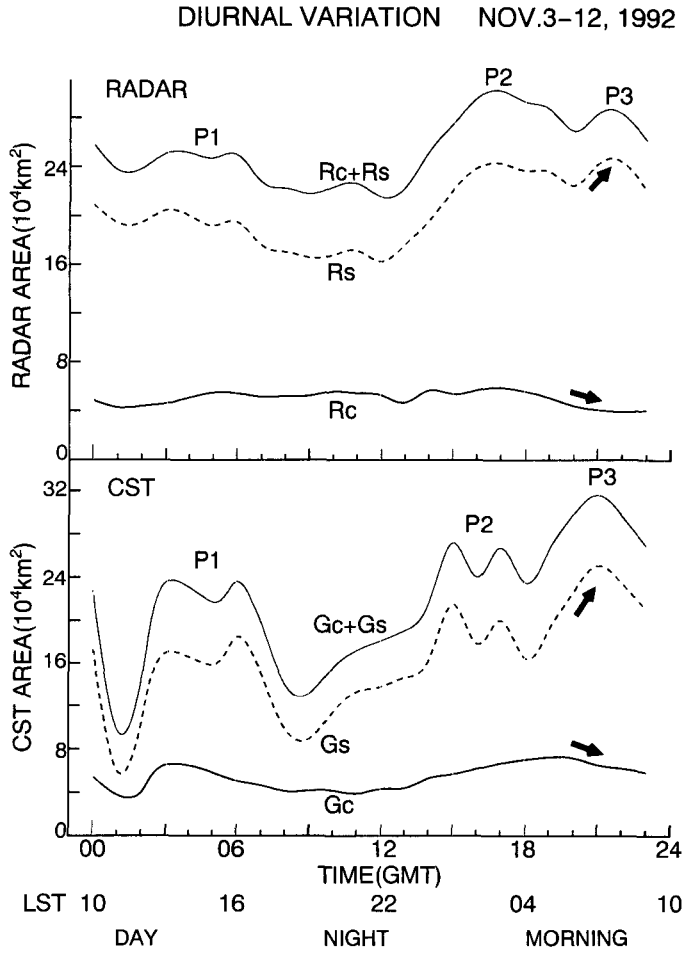

Fig. 13. Diurnal variations of the radar and CST areas of tropical convection. Area determined by radar and CST analyses are shown in the upper panel and lower panel respectively. Evening, early morning and late morning peaks are represented by P1, P2, and P3 respectively. The symbols *Rc*, *Rs*, *Gc* and *Gs* are the same as Fig. 6. Bold arrows are used to show the increase and decrease mode of the cloud area.

that the echo scattered and became weak during the late morning (P3). The former was dominated by shallow convection and isolated short-lived (~5 hours) clouds, and the latter was dominated by the stratiform anvil clouds. During the peak P2, the cloud was growing in the low altitudes ; GMS cloud not detect well though radar could. In contrast, stratiform anvil clouds developed

in the upper-troposphere which could not be well detected by radar though GMS can detect anvil clouds well. This is why the CST analyzed peak (P3) is maximum at this period. The peak period of P3 was completely consistent with the previous result of Murakami (1983) who used GMS-1 satellite data. The solid arrows in the upper and lower panels show that for both radar and CST analyses, the area of the convective component decreased while the area of stratiform component increased. This is one confirmation that P3 was dominated by anvil clouds which Murakami (1983) reported as deep convective clouds. As explained earlier, the advantage of the present analysis is to use convective and stratiform cloud components which can clearly show the exact contribution of each component. The peak P3 was about 4-6 hours later than the peak P2. At this time the stratiform components were dominant and the convective components showed a lack of dominance. This suggests that in the

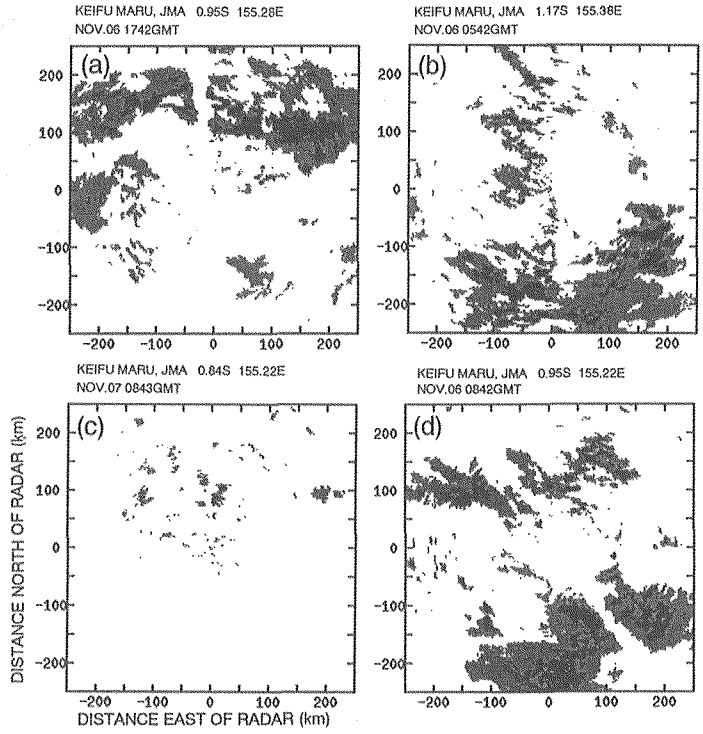

Fig. 14. Examples of peaks of a) Evening, b) Morning, c) No peak and d) Exceptional peak determined by Keifu Maru radar.

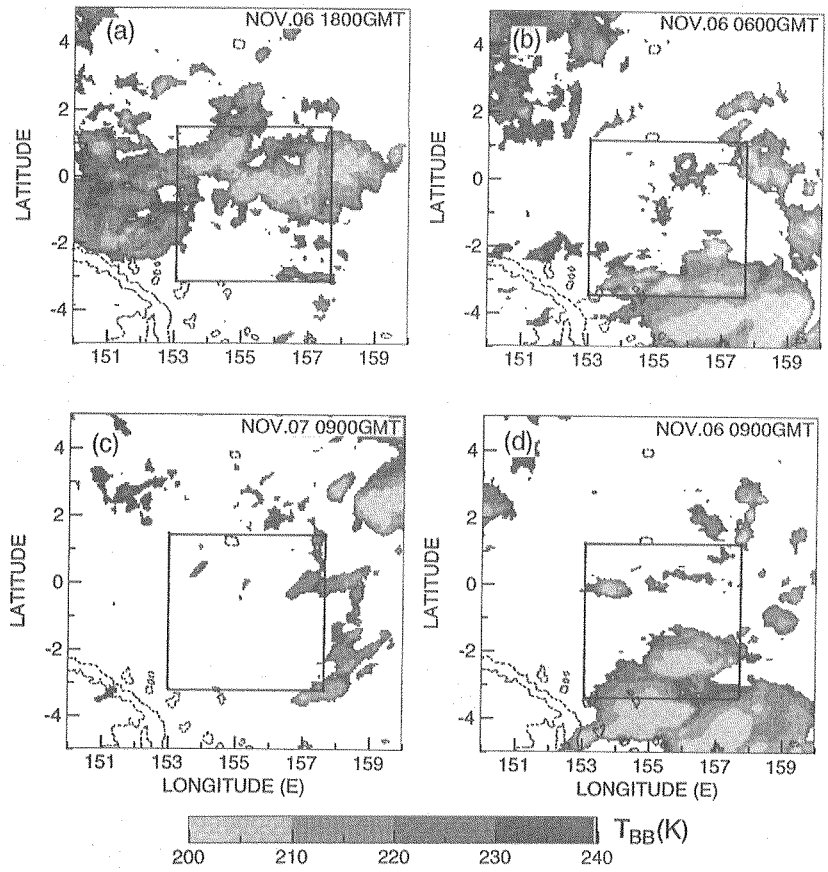

Fig. 15. Same as Fig. 14 except for GMS-IR image of large coverage (10°×10°). The radar coverage of Fig. 14 is shown by inner box (solid line) in each image. The islands are shown by dashed lines. Gray shades are used to represent cloud regions.

dissipating stage a few isolated fragments at the low-level made peak P3 suited to radar analysis while in the upper-level stratiform anvil strongly dominated to make large peak P3 suited to CST analysis. For both radar and CST analyses, suppressed activities were observed during the evening peak P1. In contrast, patterns of radar and satellite analyses were very similar. This implies the link between the cloud properties at a low altitude analyzed by radar and at the high altitude analyzed by satellite.

The examples of morning and evening peaks are shown in Figs. 14 and 15

for radar and GMS images respectively. Radar images are as follows: (a) morning peak (1742 GMT on Nov. 6); (b) evening peak (0542 GMT on Nov. 6); (c) not a peak (0843 GMT on Nov. 7); and (d) exceptional (not usual case) peak (0842 GMT on Nov. 6). The corresponding satellite images are shown with the radar coverage area denoted by a square (solid line) in each image. It is noted that the satellite image time was approximately 15 minutes ahead of radar image time. This is used for the adjustment of local time. Radar image time should be the actual local standard time (LST).

The exceptional and late morning peaks suggest that the clouds over the oceanic warm pool have a peak difference of 12-18 hours. This ten day data analysis was not sufficient for a conclusion to be reached on the diurnal variation of the tropical convection. However, this analysis is able to show the trend of 1-3 day activities due to the ~18 hour interval between the two major peaks P1 and P3 of the cloud area.

4.6 Estimation of rainfall

Daily rainfall amounts determined by radar and the CST analyses are presented in Fig. 16. It is noted that the CST rainfall amount was calculated by using the stratiform rain rate of 3.5 $mm \cdot h^{-1}$ and convective rain rate of 25 $mm \cdot h^{-1}$ as assigned from radar data. There was a good agreement between the rainfall amounts determined by both radar and CST, in Area KM. This agreemment supported the calculated amounts of rainfall in Area A and in Area B where there were no radar data. Calculation showed that precipitation determined by radar was 6.4 $m \cdot yr^{-1}$ and that determined by CST was 7.1 $m \cdot yr^{-1}$ while the expected value is 3-5 $m \cdot yr^{-1}$ (Webster and Lukas, 1992). In order to compare the results of this analysis with those of other analysis, the daily precipitation statistics is tabulated in Table 4. Keifu Maru and GMSs represent the results of this analysis. The others are the information from TOGA-COARE workshop (Bradley and Weller, 1995) except the values of Manus Island. It is seen that the precipitation estimated by Keifu Maru is a little larger than the other precipitation amounts. The Keifu Maru value is almost three times larger than the value calculated by MIT radar. This difference comes from the use of a different Z-R relationship for Keifu Maru radar than for MIT radar. Also the coverage of each radar is different, which may cause the difference in the estimation of precipitation. Further, only 10 days of active, including rainless days data were analyzed. However, precipitation at the point calculated by Paulson, and Manus rain gauge values average for only rainy days are close to the Keifu Maru value. It is seen that the GMS values are higher than

Table 4. Daily precipitation (mm) statistics.

	Cruise			Present work	IOP mean
	1	2	3		
Satellite					
SSM/I (Curry/Liu, 1995)					5.6
GPI (Arkin, 1995)					6-10
MSU (Arkin, 1995)					7.0
GMS (Area KM)				19.9 (3.2-50.4)	
GMS (Area A)				18.6 (6.2-47.0)	
GMS (Area B)				22.0 (10.9-57.2)	
Radar					
MIT 120 km (Rult et al., 1995)	4.1	5.5	5.2		5.0
MIT 150 km (Short et al., 1995)	2.8	4.6	3.2		
Keifu Maru 250 km				17.9 (1.8-57.4)	
Budget					
Frank (1995)					10.5/11.8
Lin/Johnson (1995)	4.0	7.8	4.0		5.7-6.1
Point					
ORG (McPharden, 1995)					12-14
Paulson (1995)	3.1	12.5	10.1		8.6
ORG (Bradley, 1995)	17.7	6.8			11.6
ORG (Fairall, 1995)					11.2
Rain Gauge (Manus Island)					
KITCHAPON (Uyeda et al., 1995)			6.89 (0-133)	12.44 (rainy days)	
MOMOTE (Uyeda et al., 1995)			6.61 (0-50)	12.11 (rainy days)	
BOWAT (Uyeda et al., 1995)			8.75 (0-52)	12.35 (rainy days)	

10 Nov.-10 Dec. Cruise 1, 16 Nov.-21 Jan. KITCHAPON,
12 Dec.-19 Jan. Cruise 2, 1 Nov.-27 Jan. MOMOTE,
29 Jan.-25 Feb. Cruise 3, 3 Dec.-21 Jan. BOWAT
3 Nov.-12 Nov. Present work

the other satellite values because GMS values were calibrated with Keifu Maru radar values. Therefore, when we are able to decide which radar value is appropriate it should be possible to calibrate the satellite (GMS) value to estimate the precipitation in a large domain. The advantage of the present analysis is that the convective and stratiform components for both radar and satellite analyses are individually quantified as shown in Fig. 16.

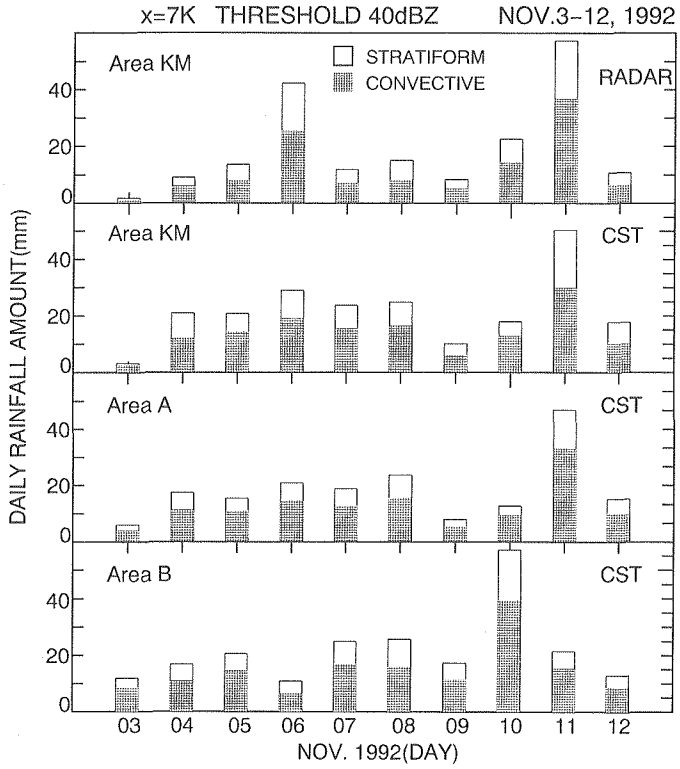

Fig. 16. Daily rainfall amounts determined by radar (upper panel) in Area KM and CST (lower three panels) in Area KM, Area A and Area B. Stratiform and convective components are divided by the threshold reflectivity of 40 dBZ.

5. Discussion

5.1 Adaption of the CST for the TOGA-COARE convection

The comparative results of radar and the CST analyses suggested that the modified CST algorithm of one geographical region is not applicable to other geographical regions without revised modifications (Kikuchi et al., 1996 ; Islam et al., 1997). If we believe that radar is one of the most reliable devices in identifiying the surface precipitation, the CST identified rainfall area is reasonable because it matched the radar identified values (Islam et al., 1997). A mismatch, however, was found in the estimation of rainfall amount. The disagreement in the rainfall estimation actually came from the underestimation of the convective rainfall amount determined by the CST even though the area was reasonable. In truth it is not necessary to obtain exactly the same amounts

of rainfall from radar and satellite data because the cloud properties in the lower-level somewhat differ from the cloud properties in the upper-level. Since there is a link between the cloud properties of the two levels (lower and upper), the important thing is to obtain comparable amounts from both of the data sets. Moreover, it is very difficult to retrieve the warm precipitation contributed by shallow convection, from satellite data. In the TOGA-COARE domain, Liu et al. (1995) also did not succeed in retrieving warm precipitation contributed by isolated small clouds by using satellite data only. In many aspects, the estimation of precipitation in a large domain is essential and satellite data is the best way to analyze it. To do this it was necessary to locate or construct a sound method for the analysis of satellite data. In this analysis, the CST algorithm was chosen because it was tested for the analyses of Florida convection (AN88), WMONEX cloud clusters (GHC90) and TOGA-COARE cloud clusters (Kikuchi and Uyeda, 1996; Islam et al., 1997). Since the use of the CST algorithm was able to determine the area as well as radar, an attempt was made to calibrate the precipitation amount determined by the CST in comparison with the precipitation amount determined by Keifu Maru radar.

Mainly this analysis followed the CST algorithm modified by GHC90 for WMONEX. As previously described, three simple modifications have been performed to adapt it in the TOGA-COARE region. First, AN88 used GOES-E data having a mesh of 8.0 km×3.1 km and GHC90 used GMS-1 data having a mesh of 5.2 km×2.1 km. The present GMS-4 CD-ROM data having a mesh of 11.1 km×11.1 km requires a correction in the equation of the slope parameter. Second, GHC90 introduced a variable x ($=7$ K) to match their result with their radar (start ≥ 1 dBZ) analysis. In order to match Keifu Maru radar (start ≥ 20 dBZ) analysis, $x=4$ K for <1 day and $x=7$ K for 10 days data analysis were determined. Third, the assignment of a rain rate was an important factor which depended on the measuring device and local environmental condition. A few cases analyzed by one C-band radar and two X-band Doppler radars identified the necessity of the correction of rain rate (Islam et al., 1997). Since there is no way to assign stratiform rain rate by CST algorithm, and convective rain rate depends on the environmental condition, rain rate was assigned from radar analysis. The assigned rain rates ($>11.53\ \mathrm{mm\cdot h^{-1}}$ ($=40$ dBZ) as convective and $\leq 11.53\ \mathrm{mm\cdot h^{-1}}$ as stratiform) successfully separated the convective and stratiform components. Using these assigned rates consistent results with other works (e.g., Houze, 1977; Cheng and Houze, 1979; Steiner and Houze, 1993; Liu et al., 1995) were obtained. This analysis is a reminder that the use of x value in the CST algorithm varies for each case depending on

the length of the period of analysis. Therefore, care should be taken in determing the x value which should be depend on the interest of the application.

5.2 *Cloud properties in the lower-level and upper-level*

The CST identified a precipitable portion of the clouds defined by the enclosed boundary of 230 K in T_{BB} (Islam et al. 1998) is shown in Fig. 17. Averaging all three analyzed areas (KM, A, and B), the CST ($x=7$ K) identified 56% of the cloud as precipitable portion ; 44% was nonprecipitable. According to Liu et al. (1995), the precipitable portion was only 15% and the nonprecipitable portion was 85%. This large difference stems from two causes : first, the present analysis used a cloud boundary with the adjustment of Ts value to extract the precipitable portion, while Liu's analysis used the high cloud top temperature that extended below freezing level ; second, their cloud classification scheme does not work well for warm, precipitating and isolated small clouds due to their large grid size (50 km×50 km), and this analysis used

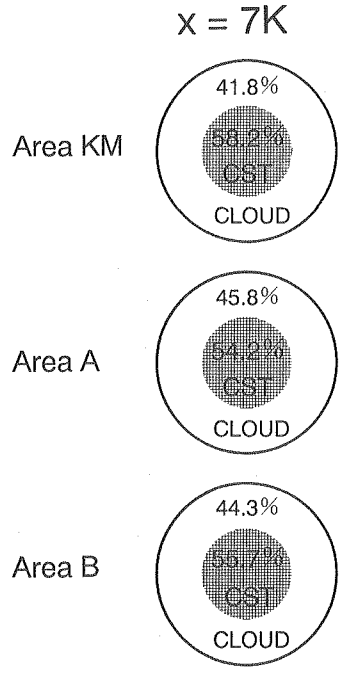

Fig. 17. Precipitable portions of the cloud determined by the CST for Area KM, Area A and Area B. The cloud is determined by the enclosed boundary of T_{BB} of 230K. Shaded regions are the precipitable portion of the defined cloud.

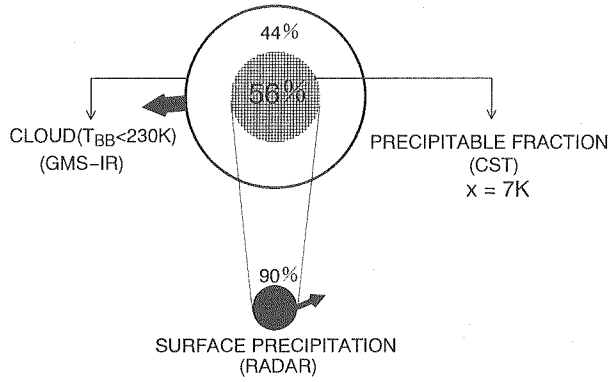

Fig. 18. Schematic illustration for the movement direction of cloud, precipitation determined by CST and radar echo. The precipitable portion of the cloud is determined by CST and surface precipitation is determined by radar for 10 days from November 3, 1992.

the small grid size (11.1 km×11.1 km) to resolve small cloud.

Similarities and dissimilarities were also observed between radar and satellite analyses. Low-level warm rain contributed by a small shallow convection was observed in the analysis of radar data (Fig. 10). It was not found in the analysis of satellite data (Fig. 11) because the satellite detected the convective cloud when its top was tall enough and extended above the freezing level (0°C). Both radar and satellite data showed similar patterns of the linear relationship for the stratiform anvil cloud. As shown in Fig. 18, the surface precipitation calculated by radar was 90% of the precipitable portion (56%) of the cloud that was calculated by the CST. These results show the good adjustment between precipitations in the lower-level and upper-level.

5.3 Contribution of convective and stratiform precipitations

The quantifications of convective and stratiform precipitations are important in themselves as well as for their intimate relationship with water budget, estimation of imported moisture and the determination of sea surface temperature. In order to estimate the precipitation contributed from convective and stratiform cloud components individually, a threshold reflectivity of 40 dBZ for Keifu Maru radar is defined (section *4.2*) to separate them. The defined threshold reflectivity well separated the convective (62%) and stratiform (38%) rainfall amounts in the Keifu Maru radar analysis. The final calculation showed that the CST determined rainfall amounts were G_S=36% and G_C=64% which are

almost the same as the radar values. The stratiform component is consistent with the results of GATE (Houze, 1977; Cheng and Houze, 1979) and TOGA-COARE (Liu et al., 1995; Kikuchi and Uyeda, 1996). The convective component is consistent with the result of TOGA-COARE (Williams et al., 1995). They calculated 68% of the rain from convective-type (combination of convective and mixed stratiform/convective) clouds by using Doppler wind profiler data collected in Manus Island. The accumulated ten day (Nov. 3-12, 1992) rainfall amounts were 4.5×10^{13} kg for radar and 5.0×10^{13} kg for CST. One may expect a higher CST value than this obtained value. But our main interest is the link between the surface precipitation determined by radar and the precipitation of higher altitude determined by satellite. So the CST value was calibrated with the radar value. However, the CST estimated rainfall amount is 1.11 times the radar estimated rainfall amount. This supports the chance of assigning the rain rate to divide convective and stratiform components and to use the radar rain rate for analysis of satellite data. The quantification of the individual rainfall amount was very important because the tropical MCSs are composed of both convective and stratiform clouds. Recently, there are many works on this separation process though to date it is not appropriately quantified.

As explained in Table 4, the estimated value was somewhat larger because only a 10 day active period data was used and the reflectivity of Keifu Maru radar data may be too large. It should be noted that Keifu Maru radar reflectivity is not calibrated yet. Calibrated radar data is essential to estimate appropriate precipitation from both radar and satellite data. In the future when well calibrated radar data is available then satellite (GMS) data should be useful after the performance of simple adjustment with radar results.

In the above calculation of the precipitation, a single Z-R relationship was used to convert radar reflectivity into rain rate. Using separate Z-R relations for convective and stratiform precipitation areas, Steiner and Houze (1993) calculted 57%-69% as convective rain of the total rain. They used different Z-R relations from the present study. Though both results are close, it is hard to state which is the appropriate one. The correct identification of every convective feature might be impossible, but to find the most consistent and the best possible way of dividing convective and stratiform cloud components is one of the objectives of this work. In the next step it may be possible to verify this procedure by using separate Z-R relations for convective and stratiform cloud components and comparing the results of radar and CST analyses.

5.4 Other features

A number of clouds interacted between themselves to form a cloud cluster. The size of the clouds and cloud clusters at different stages are important in detecting their impacts on radiative fluxes and the climate change. The rainfall regimes are objectively separated to understand the size of the clouds at different stages. As was found, the echo length (L) ranges were formative: $L<100$ km; mature: $100<L<330$ km; and dissipating: $L>330$ km. These were used to calculate the cloud area and fractional coverage at the individual stage. The fractional coverage of convective and stratiform components were found to be 25% and 75% respectively, while precipitation amounts were estimated 64%-68% and 36%-38% respectively.

The diurnal variation of the tropical convecion was examined using radar and satellite data. In this work the separated convective and stratiform cloud components were used for both radar and satellite analyses. These components gave clear explanations and disclosed the link between the properties of the lower and upper atmospheres. Three peaks were found: an evening peak, an early morning peak, and a late morning peak. The interval between peak P1 and peak P2/P3 was 12-18 hours. This is important in explaining the 1-3 days activities of tropical cloud clusters. The analysis of three peaks in a day differs from the conventional explanation of two peaks (Murakami 1983). The early morning peak (P2) was contributed to the small shallow convection and isolated clouds which occurred at around 2-3 LST. These small clouds organized and transformed to form the late morning peak which occurred at around 6-8 LST. The late morning peak (P3) came from the contribution of stratiform cloud components which were small for radar analysis and too large for CST analysis. The enhancement of this peak could not resolve without the separation of convective and stratiform components. Exceptional peaks which were often observed during the study period support the continuation of the activities longer than one day.

6. Conclusions

Since the MCSs were composed of both convective and stratiform components, it was necessary to separate them both in radar and satellite images. A threshold reflectivity of 40 dBZ was determined for Keifu Maru radar to separate convective and stratiform cloud components. This threshold separated the cloud components to well obtain conformance with the result of satellite analy-

sis. The stages of the tropical clouds were objectively separated by length (L) ranges as follows: (1) formative: $L<100$ km; (2) mature: $100<L<330$ km; and (3) dissipating: $L>330$ km. The size at different stages estimated from the length at particular stage may be useful as input to the model calculations. Through the above analysis, knowledge of the properties of cloud clusters has been expanded. Four convective activities were observed having the duration of 1-3 days.

To better analyze the above properties improvement of the CST algorithm was needed for the TOGA-COARE domain. In order to adapt the CST in this analysis, simple modifications were performed on the: (1) calculation of the slope parameter; (2) determination of the stratiform threshold temperature; and (3) assignment of both convective and stratiform rain rates from Keifu Maru radar analysis. The assigned convective and stratiform rain rates were 25 mm·h^{-1} and 3.5 mm·h^{-1} respectively.

The cloud areas covered by convective and stratiform regions were 25% and 75% respectively. In contrast, convective components occupied a small portion at the center of the cloud while convective portion surrounded by stratiform large anvil occupied the rest. Precipitation falling from convective components was determined to be 62% by radar and 64% by CST. The large amount of convective parts were related to the warmness of the SST over the western Pacific warm pool. The stratiform precipitation which fell from the anvil cloud was accounted for as 38% by radar and 36% by CST. These values were well consistent with the results of GATE (Houze, 1977; Cheng and Houze, 1979) and TOGA-COARE (Liu et al., 1995; Kikuchi and Uyeda, 1996). The modified CST was used to estimate precipitation from satellite data in addition to radar data: 56% of the defined (by $T_{BB}=230$ K; Islam et al., 1998) cloud was found to be precipitable while 44% was nonprecipitable. Further work is necessary to verify this percentage. It should be noted that isolated small clouds greatly contributed to this precipitating portion, so the verification method must have the ability to detect isolated small clouds. The annual precipitation accounted for by radar was 6.4 mm·yr^{-1} and for CST was 7.1 mm·yr^{-1}. As previously commented, these values were somewhat large due to the short-active-period data analysis and large reflectivity of Keifu Maru radar. However, estimated precipitation will be helpful in projecting water budgets and in estimating imported moisture in this region.

By applying an appropriately modified version of the GHC90's CST to GMS-IR imagery, the present analysis is able to conclude that in the future it may be possible to estimate approximate precipitation by using satellite data for

a large domain when calibrated radar data for a long period is available. The successful adaption of GHC's CST to TOGA-COARE cloud cluster provides encouragement for the future application of this method to the tropical cloud clusters. As an example, TRMM (Tropical Rainfall Measuring Mission, launched in 1997) is one where this method might be applicable. The use of a separate Z-R relation to calculate convective and stratiform rain rates, for the verification of the assigned values used in this study, is also suggested for future study.

Acknowledgments

The authors would like to express their thanks to the JMA for providing Keifu Maru radar data. Special thanks to Dr. N. Takahashi of Communication Research Laboratory, Dr. R. Oki of the University of Tokyo and M. Katsumata of Hokkaido University for help in data reading. One of the authors M.N. Islam was supported by the Japanese Government (Monbusho) Scholarship from the Ministry of Education, Science, Sports and Culture of Japan during this study. This study was partly supported by the Grant-in-Aid (No. 09640514) of the Ministry of Education, Science, Sports and Culture of Japan.

References

Adler, R.F. and A.J. Negri, 1988. A satellite infrared technique to estimate tropical convective and stratiform rainfall. J. Appl. Meteor., **27**, 30-51.

Adler, R.F. and R.A. Mack, 1984. Thunderstorm cloud height-rainfall rate relations for use with satellite rainfall estimation techniques. J. Clim. Appl. Meteor., **23**, 280-296.

Austin, P.M., S. Geotis, J. Cunning, J. Thomas, T.R. Sax and J. Gillespie, 1976. Raindrop size distributions and Z-R relationship for GATE. Abstract in Bull. Amer. Meteor. Soc., **57**, 518.

Battan, L.J., 1973. Radar Observation of the Atmosphere. The University of Chicago Press, 324 pp.

Bradley, F. and R. Weller (ed.), 1995. Joint workshop of the TOGA-COARE flux and atmosphere working groups. Boulder, Colorado, USA, 11-13 July, 14 pp.

Cheng, C.-P. and R.A. Houze, Jr., 1979. The distribution of convective and mesoscale precipitation in GATE radar echo patterns. Mon. Wea. Rev., **107**, 1370-1381.

Churchill, D.D. and R.A. Houze, Jr., 1984a. Development and structure of winter monsoon cloud clusters on 10 December 1978. J. Atmos. Sci., **41**, 933-960.

Gamache, J.F. and R.A. Houze, Jr., 1982. Mesoscale air motions associated with a tropical squall line. Mon. Wea. Rev., **110**, 118-135.

Goldenberg, S.B., R.A. Houze, Jr. and D.D. Churchill, 1990. Convective and stratiform components of a winter monsoon cloud cluster determined from geosynchronous infrared satellite data. J. Meteor. Soc. Japan, **68**, 37-63.

Houze, Jr., R.A., 1977. Structure and dynamics of a tropical squall-line system. Mon. Wea.

Rev., **105**, 1540-1567.
Houze, Jr., R.A. and P.V. Hobbs, 1982. Organization and structure of precipitating cloud systems. Advances in Geophysics, **41**, 3405-3411.
Houze, R.A., Jr. and E.N. Rappaport, 1984. Air motions and precipitation structure of an early summer squall line over the eastern tropical Atlantic. J. Atmos. Sci., **41**, 553-574.
Islam, M.N., H. Uyeda, O. Kikuchi and K. Kikuchi, 1996. Characteristics of clouds, cloud clusters and a supercluster observed on November 11-12 during the TOGA-COARE IOP. Preprints: 12th International Conference on Clouds and Precipitation, Zurich, 546-549.
Islam, M.N., H. Uyeda and K. Kikuchi, 1997. Characteristics of clouds and cloud clusters obtained by radar and satellite data during the TOGA-COARE IOP. J. Fac. Sci. Hokkaido Univ., Ser. VII(Geophysics), **10**, 189-223..
Islam, M.N., H. Uyeda and K. Kikuchi, 1998. Cloud clusters and a supercluster analyzed with radar and satellite data during the TOGA-COARE IOP. J. Meteor. Soc. Japan (in preperation).
Kikuchi, O. and H. Uyeda, 1996. Doppler radar observations on the structure and characteristics of tropical clouds during TOGA-COARE IOP in Manus, Papua New Guinea: Characteristics of cloud clusters analyzed with Doppler radar and GMS-IR data. J. Fac. Sci. Hokkaido Univ., Ser. VII (Geophysics), **10**, 107-133.
Leary, C.A., 1984. Precipitation structure of the cloud clusters in a tropical easterly wave. Mon. Wea. Rev., **112**, 313-325.
Leary, C.A. and R.A. Houze, Jr., 1979. The structure and evolution of convection in a tropical cloud cluster. J. Atmos. Sci., **36**, 437-457.
Leary, C.A. and E.N. Rappaport, 1987. The life cycle and internal structure of a mesoscale convective complex. Mon. Wea. Rev., **115**, 1503-1527.
Liu, G., J.A. Curry and R.S. Sheu, 1995. Classification of clouds over the western equatorial Pacific Ocean using combined infrared and microwave satellite data 1995. J. Geophys. Res., **100**, 13811-13826.
Machado, L.A.T. and W.B. Rossow, 1993. Structural characteristics and radiative properties of tropical cloud clusters. Mon. Wea. Rev., **121**, 3234-3260.
Marshall, J.S. and W.M. Palmer, 1948. The distribution of raindrops with size. Jour. Meteor., **5**, 16-18.
Mori, K., 1992. Internal structure and time evolution of a cloud cluster in the western tropical Pacific region observed by Keifu Maru. J. Meteor. Soc. Japan, **70**, 1111-1123.
Mori, K., 1995. Equatorial convection observed by research vessel Keifu Maru during the TOGA COARE IOP, November 1992. J. Meteor. Soc. Japan, **73**, 491-508.
Murakami, M., 1983. Analysis of the deep convective activity over the western Pacific and Southeast Asia. Part I: Diurnal variation. J. Meteor. Soc. Japan, **61**, 60-75.
Rappaport, E.N., 1982. Structure and dynamics and a typical tropical squall-line system. M.S. thesis, 266 pp., University of Wash., Seattle.
Smith, J.A., 1993. Marked point process models of raindrop-size distributions. J. Appl. Meteor., **32**, 284-296.
Steiner, M. and R.A. Houze, Jr., 1993. Three-dimensional validation at TRMM ground truth sites: Some early results from Darwin, Australia. Preprints: 26th Conference on Radar Meteorology, Norman, OK, Amer. Meteor. Soc., 417-420.
Steiner, M., R.A. Houze, Jr. and S.E. Yuter, 1995. Climatological characterization of three-dimensional storm structure from operational radar and rain gauge data. J. Appl. Meteor., **34**, 1978-2007.
Takahashi, N. and H. Uyeda, 1995. Doppler radar observation of the structure and characteristics of tropical clouds during the — TOGA-COARE IOP in Manus, Papua New

Guinea : Three case studies on November 23 and December 16, 1992 —. J. Meteor. Soc. Japan, **73**, 427-442.

Uyeda, H., Y. Asuma, N. Takahashi, S. Shimizu, O. Kikuchi, A. Kinoshita, S. Matsuoka, M. Katsumata, K. Takeuchi, T. Endoh, M. Ohi, S. Satoh, Y. Tachibana, T. Ushiyama, Y. Fujiyoshi, R. Shirooka, N. Nishi, T. Tomita, H. Ueda, T. Sueda and A. Sumi, 1995. Doppler radar observations on the structure and characteristics of tropical clouds during the TOGA-COARE IOP in Manus, Papua New Guinea — Outline of the observation —. J. Meteor. Soc. Japan, **73**, 415-426.

Webster, P.J. and R. Lukas, 1992. TOGA COARE : the coupled ocean-atmosphere response experiment. Bull. Amer. Meteor. Soc., **72**, 1481-1505.

Williams, C.R., W.L. Ecklund and K.S. Gage, 1995. Classification of precipitating clouds in the tropics using 915-MHz wind profilers. J. Atmos. Oceanic Technol., **12**, 996-1012.

Woodley, W.L., 1970. Precipitation results from a pyrotechnique cumulus seeding experiment. J. Appl. Meteor., **9**, 242-257.